nature structural & molecular biology

A molecular chaperone breaks the catalytic cycle that generates toxic Aβ oligomers

Samuel I A Cohen[1,6], Paolo Arosio[1,6], Jenny Presto[2,6], Firoz Roshan Kurudenkandy[2], Henrik Biverstål[2], Lisa Dolfe[2], Christopher Dunning[3], Xiaoting Yang[3], Birgitta Frohm[3], Michele Vendruscolo[1], Jan Johansson[2,4,5], Christopher M Dobson[1], André Fisahn[2], Tuomas P J Knowles[1] & Sara Linse[3]

Alzheimer's disease is an increasingly prevalent neurodegenerative disorder whose pathogenesis has been associated with aggregation of the amyloid-β peptide (Aβ42). Recent studies have revealed that once Aβ42 fibrils are generated, their surfaces effectively catalyze the formation of neurotoxic oligomers. Here we show that a molecular chaperone, a human Brichos domain, can specifically inhibit this catalytic cycle and limit human Aβ42 toxicity. We demonstrate *in vitro* that Brichos achieves this inhibition by binding to the surfaces of fibrils, thereby redirecting the aggregation reaction to a pathway that involves minimal formation of toxic oligomeric intermediates. We verify that this mechanism occurs in living mouse brain tissue by cytotoxicity and electrophysiology experiments. These results reveal that molecular chaperones can help maintain protein homeostasis by selectively suppressing critical microscopic steps within the complex reaction pathways responsible for the toxic effects of protein misfolding and aggregation.

Alzheimer's disease (AD) is a progressive and fatal neurodegenerative disorder characterized by memory loss and personality changes[1–5]. This disease is one of over 40 amyloid-related disorders[6–8], which also include Parkinson's and Huntington's diseases. This class of disorders is associated with the misfolding of specific peptides or proteins and the subsequent formation of ordered amyloid fibrils having a common cross-β structure[6,7,9–11]. A central molecular species in AD is the 42-residue amyloid-β peptide, Aβ42, which is the dominant component of the plaques that are a defining histopathological characteristic of the brains of patients with AD[4]. Studies over the past decade, however, have indicated that it is the prefibrillar oligomeric aggregates of amyloidogenic peptides and proteins such as Aβ42 that are likely to be the major toxic agents causing neuronal cell death[3,12–14].

Major advances have recently been made in understanding the molecular mechanisms that lead to the generation of such toxic oligomers. This problem is highly complex because the process of peptide and protein aggregation involves multiple events occurring simultaneously in a multistep nucleated polymerization reaction[15–18] that results in the formation of high-molecular-weight fibrillar aggregates from the soluble monomeric peptide via nonfibrillar oligomeric species[19–22]. In this type of reaction, the homogeneous primary nucleation[21–24] of new oligomers from monomers is inherently a slow process, and it is therefore unlikely to generally represent the major origin of toxicity. It has been shown, however, that the production of oligomers can be catalyzed in a very effective manner by the surfaces of high-molecular-weight fibrillar aggregates[19]. This catalytic pathway takes the form of a secondary nucleation reaction[25–27] involving both free monomers and fibrils, and it can dramatically increase the overall rate of Aβ42 aggregation and oligomer formation[19,28,29]. As such, although not directly toxic themselves, Aβ42 fibrils provide a catalytic surface for the continuous generation of toxic oligomers, species that can also grow and convert into additional fibrils[19,21,30], thus further promoting the formation of additional toxic species in a catalytic cycle. The fibrils, therefore, play a key part in the formation of oligomers by lowering the kinetic barriers that under normal circumstances hinder *de novo* formation.

Because of the importance of the catalytic cycle in the production of Aβ42 oligomers, an attractive strategy to prevent the formation of these damaging assemblies would be the identification of inhibitors that can interfere with the catalytic activity of the fibril surfaces; however, no agents with this specific effect have yet been identified. To explore the potential of this strategy, we describe the effect of the chaperone domain Brichos[31] on the molecular mechanism underlying the aggregation of Aβ42. Molecular chaperones have been known for several decades to have key roles in aiding in folding *in vivo* of newly synthesized proteins into their native states, in trafficking proteins to specific locations in cells and in facilitating the efficient assembly of molecular subunits into functional multimeric structures[32–34]. Moreover, it is increasingly evident that the chaperone machinery plays an important part in maintaining

[1]Department of Chemistry, University of Cambridge, Cambridge, UK. [2]Department of Neurobiology, Care Sciences and Society, Center for Alzheimer Research, Division of Neurogeriatrics, Karolinska Institutet, Stockholm, Sweden. [3]Department of Biochemistry and Structural Biology, Lund University, Lund, Sweden. [4]Department of Anatomy, Physiology and Biochemistry, Swedish University of Agricultural Sciences, Uppsala, Sweden. [5]Institute of Mathematics and Natural Sciences, Tallinn University, Tallinn, Estonia. [6]These authors contributed equally to this work. Correspondence should be addressed to A.F. (andre.fisahn@ki.se), T.P.J.K. (tpjk2@cam.ac.uk) or S.L. (sara.linse@biochemistry.lu.se).

Received 17 August 2014; accepted 8 January 2015; published online 16 February 2015; doi:10.1038/nsmb.2971

protein homeostasis under a wide range of circumstances[33,35]. Several pathways, including chaperone-mediated disaggregation and stimulation of proteolyic degradation, have been identified as part of a complex network that regulates proteostasis[33,34,36]. In particular, a range of genetic and biochemical studies have implied that chaperones have a critical protective role in relation to the aberrant protein aggregation processes associated with protein misfolding disorders[6,7,33,37–42], although much remains to be established concerning the precise mechanisms of action of such processes.

Brichos, a protein domain of approximately 100 amino acids, was initially identified in the proteins Bri, related to familial British dementia, chondromodulin, associated with chondrosarcoma and lung surfactant C precursor protein (proSP-C)[43] and has now been found in approximately ten distantly related protein families[44–46]. Brichos domains have been found experimentally to inhibit misfolding and aggregation both *in vitro*[31,47] and *in vivo*[48,49], and mutations in proteins containing Brichos domains have been linked to a variety of forms of amyloid disease[50,51]. Here we reveal the mechanism by which Brichos performs its antiaggregation function on Aβ42 and show that this molecular chaperone interferes highly selectively and dramatically with the key secondary nucleation reaction. Brichos is therefore an effective inhibitor of the catalytic mechanism underlying Aβ42 aggregation, and it can consequently suppress the toxicity associated with the aggregation reaction. Our results thus reveal that molecular chaperones possess capabilities that go well beyond their established ability to interact directly with aggregation-prone species in solution[2,32–34] and that they are able to suppress the toxicity associated with aggregation reactions by interacting with amyloid fibrils selectively to break the critical catalytic cycle through which toxic oligomers are generated.

RESULTS

Brichos inhibits surface-catalyzed secondary nucleation of Aβ42

We first monitored the kinetics of the aggregation of Aβ42 under the quiescent conditions described previously[19,20] and obtained data completely consistent with our earlier studies. In order to establish well-defined initial conditions for the kinetic experiments, and hence to obtain reproducible data, we purified the recombinant monomeric Aβ42 peptide to very high levels by repeated applications of size-exclusion chromatography and carefully controlled the inertness of surfaces with which it made contact[20]. Upon addition of the Brichos domain from proSP-C[51], at concentrations between 10% and 100% Aβ42 monomer equivalents, we observed a reduction in the overall rate of formation of fibrils and characteristic changes in the time course of the reaction (**Fig. 1** and **Supplementary Fig. 1**). To connect these observations with the underlying microscopic mechanisms that contribute to the macroscopic changes, we used an analytical approach to predict the effects of perturbing the different individual microscopic processes involved in Aβ42 aggregation on the global kinetics of aggregation[52]. Specifically, we predicted alterations in the rates of primary nucleation, fibril elongation and secondary nucleation to result in distinct and characteristic changes in the shapes of the reaction profiles (**Fig. 1**).

Because all of the rate constants associated with the aggregation pathway of Aβ42 are known[19], we can quantitatively predict the effects on the reaction profile accompanying any given perturbation, for example, the inhibition of individual molecular steps (**Fig. 1a–c**, green dashed lines), without introducing any additional fitting parameters. In particular, the effects of the complete inhibition of secondary nucleation can be predicted (**Fig. 1c**, green dashed line) simply by setting the rate constant of this process to zero in the integrated rate law[19] that describes Aβ42 aggregation (**Supplementary Fig. 2**; rate law in **Supplementary Note**). Remarkably, in the presence of an excess of the Brichos domain, the data at all times precisely match the predictions for complete inhibition of secondary nucleation—but match none of the other mechanisms of inhibition that we tested by reducing the corresponding rate constants—thus revealing that this molecular chaperone acts specifically to completely inhibit this microscopic step in the aggregation reaction. In order to test whether or not this specificity of action (i.e., the selective inhibition of secondary nucleation) is a ubiquitous characteristic shared with other proteins,

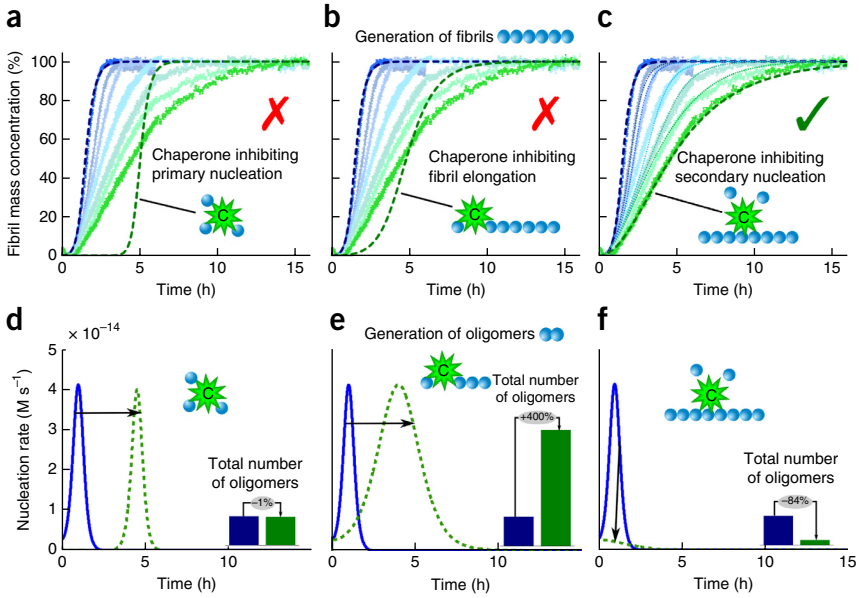

Figure 1 Kinetics of Aβ42 aggregation in the presence of Brichos. (**a–c**) Reaction profiles for aggregation in the absence of Brichos and in the presence of 10%, 15%, 35%, 50%, 75% and 100% Aβ42 monomer equivalents of Brichos, from left (blue) to right (green) respectively. The data show averages (points) and standard errors over five technical replicates. The effect of Brichos saturates at a stoichiometry of approximately one monomer equivalent of Aβ42 (**Supplementary Fig. 1**). The blue dashed line is the integrated rate law for Aβ42 aggregation in the absence of Brichos, according to the rate constants determined previously[19]. The green dashed lines show predictions for the resulting reaction profiles when primary nucleation (**a**), fibril elongation (**b**) and secondary nucleation (**c**) are inhibited by the chaperone (**Supplementary Fig. 2**). The thin dotted lines in (**c**) are theoretical predictions for the reaction profiles at the intermediate Brichos concentrations using the association and dissociation rate constants determined for its binding by SPR (**Fig. 3b**). In schematics, C, chaperone; blue spheres, Aβ42. (**d–f**) Time evolution of the nucleation rate calculated from the kinetic analysis. The blue line corresponds to the situation in the absence of Brichos, and the green dashed lines show predictions for the cases in which primary nucleation (**d**), fibril elongation (**e**) or secondary nucleation (**f**) are each inhibited by the chaperone. The insets show the relative numbers of oligomers generated during the aggregation reaction. The concentration of monomeric Aβ42 was 3 μM.

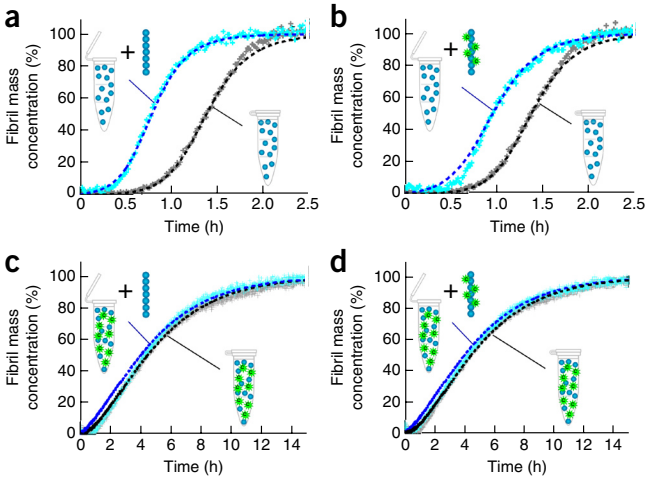

Figure 2 Inhibition by Brichos of Aβ42 surface-catalyzed secondary nucleation of oligomers. (**a**–**d**) Kinetics of aggregation upon addition of preformed Aβ42 fibrils, grown in the absence (**a**,**c**) or presence (**b**,**d**) of Brichos, to monomeric Aβ42 with (**c**,**d**) or without (**a**,**b**) Brichos in solution. Fibrils grown in the presence of Brichos (**b**) do not accelerate the reaction to the same extent as fibrils that have never been exposed to Brichos (**a**), thus showing that Brichos binds to fibrils. Addition of Brichos to solutions in which aggregation was underway (**c**,**d**) arrested the reaction and prevented the acceleration due to added fibrils, even with fibrils grown in the absence of chaperone. The dashed lines show predictions[19] for the reaction profiles with the secondary nucleation rate constant set to the value measured previously in the absence of the chaperone[19] (**a**), 60% of this value (**b**) or zero (**c**,**d**). The solution concentrations of Aβ42 and Brichos were 3 μM; the concentration of preformed fibrils was 6 nM. All data show four technical replicates overlaid.

we performed experiments in which we probed the aggregation of the Aβ42 peptide in the presence of a range of diverse control proteins, including calbindin D9k, calmodulin, the B1 domain of protein G and human serum albumin. These measurements revealed that none of these proteins interfered with Aβ42 aggregation in the same manner as Brichos (**Supplementary Fig. 3**).

A reduction in the rate of primary nucleation, fibril elongation or secondary nucleation does not significantly affect the total quantity of mature fibrils formed over the duration of the Aβ42 aggregation reaction because in all cases the soluble peptide is eventually converted almost entirely into fibrils[19,20]. Critically, however, kinetic analysis (**Fig. 1d**–**f**) reveals that the specific inhibition of each of the microscopic processes not only will change the time at which the plateau in the reaction profile of aggregation occurs but also will have very different effects on the generation of oligomers during the reaction. In particular, the reduction of the rate of primary nucleation delays the aggregation reaction (**Fig. 1d**) but does not change the total number of oligomers generated during the reaction, whereas the specific inhibition of the elongation process redirects the reactive flux involved in the conversion of the monomeric species to the fibrillar state toward secondary nucleation processes, therefore dramatically increasing the number of new oligomers that are generated (**Fig. 1e**). By contrast, suppressing the secondary nucleation process directs the reaction pathway toward elongation events, thereby almost entirely preventing the generation of oligomers (**Fig. 1f**). This analysis therefore predicts that the specific inhibition of secondary nucleation events, identified here for the Brichos domain, is an extremely effective strategy for preventing the formation of low-molecular-weight oligomeric species and hence for dramatically reducing the toxicity associated with the aggregation reaction. Conversely, simply inhibiting the rate of elongation of fibrils would increase the concentration of toxic species and hence increase rather than decrease the toxicity associated with the aggregation process.

Brichos interacts specifically with fibrillar but not monomeric Aβ42

Inhibition of secondary nucleation requires perturbation of the interactions between soluble monomers and amyloid fibrils, and in principle either species could be targeted by Brichos. To identify the molecular species on which this molecular chaperone acts, we therefore performed experiments in which newly formed Aβ42 fibrils, produced in the presence or absence of Brichos, were diluted and added to freshly prepared monomer solutions and then also incubated in the presence and absence of Brichos (**Fig. 2**). We observed that pristine fibrils that had not been exposed to the chaperone at any stage enhance the process of secondary nucleation and increase the rate of aggregation (ref. 19 and **Fig. 2a**). By contrast, we have found in the present work that preformed fibrils that had been generated in the presence of Brichos (**Fig. 2b**) accelerate aggregation, even in the absence of Brichos in solution, to a markedly smaller extent than do fibrils formed in the absence of chaperone (**Fig. 2a**). Indeed, the kinetic analysis indicates a reduction of approximately 40% in the secondary nucleation rate in this latter case (**Fig. 2b**), showing that a substantial fraction of the chaperones must have remained bound to the fibrils during the time course of the aggregation reaction. Furthermore, we observed the surface catalytic activity of fibrils to be entirely abolished when we brought preformed aggregates generated in the absence of molecular chaperones into contact with solutions containing both Brichos and monomeric Aβ42 at equal stoichiometry (**Fig. 2c**), thus demonstrating the ability of Brichos to arrest even ongoing reactions. We obtained identical results when adding fibrils formed in the presence of Brichos to solutions containing both monomeric Aβ42 and Brichos (**Fig. 2d**). These results are consistent with previous observations that Brichos is able to arrest ongoing Aβ42 and Aβ40 aggregation reactions when added at various time points[31].

The kinetic data with and without preformed seed fibrils suggest a mechanism for inhibition of aggregation involving the noncovalent association of Brichos with Aβ42 fibrils. To probe this mechanism further, we used transmission electron microscopy (TEM) with nanogold-conjugated anti-Brichos antibodies. The resulting images (**Fig. 3a**) provide a striking visualization of the nature of the interactions and clearly reveal specific binding of Brichos along the fibril surface. We also

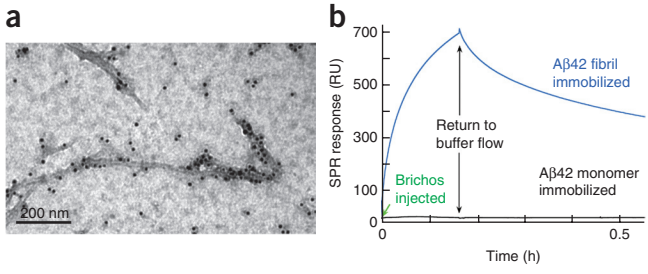

Figure 3 Brichos interacts with fibrillar but not monomeric Aβ42. (**a**) TEM images with a nanogold-conjugated secondary antibody against Brichos, showing binding of the chaperone to Aβ42 fibrils. (**b**) SPR analysis verifying specific binding to fibrils, allowing determination of the association ($k_{on} \approx 5.1 \times 10^3$ M^{-1} s^{-1}) and dissociation ($k_{off} \approx 2.1 \times 10^{-4}$ s^{-1}) rate constants and implying an apparent $K_d \approx 40$ nM. No binding was detected to the monomer or to control in the absence of Aβ42. 1 response unit (RU) = 1 pg mm^{-2}.

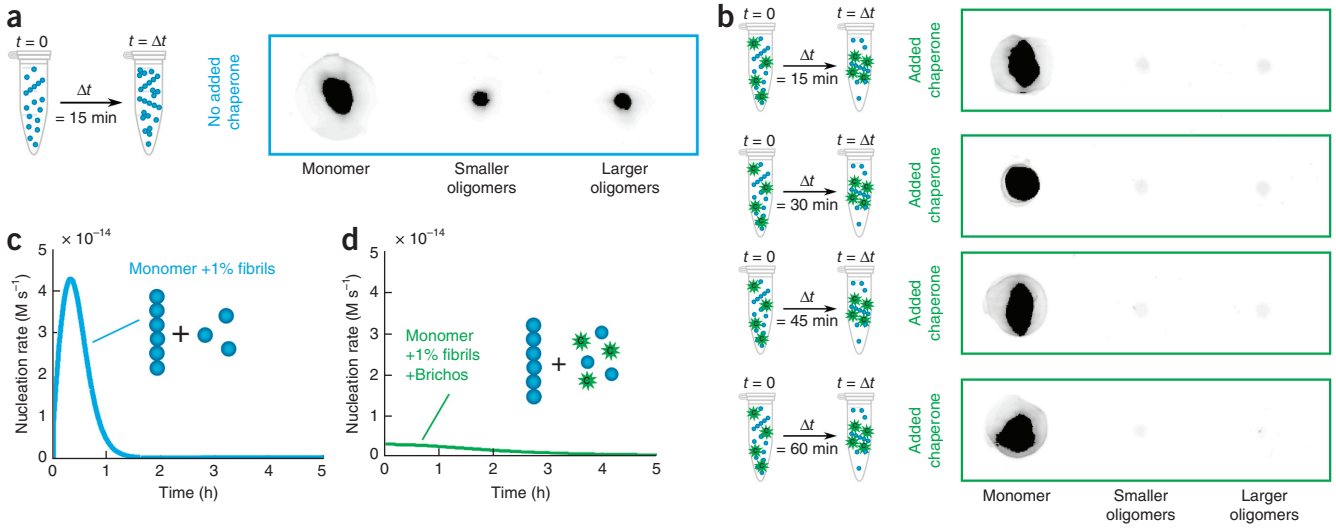

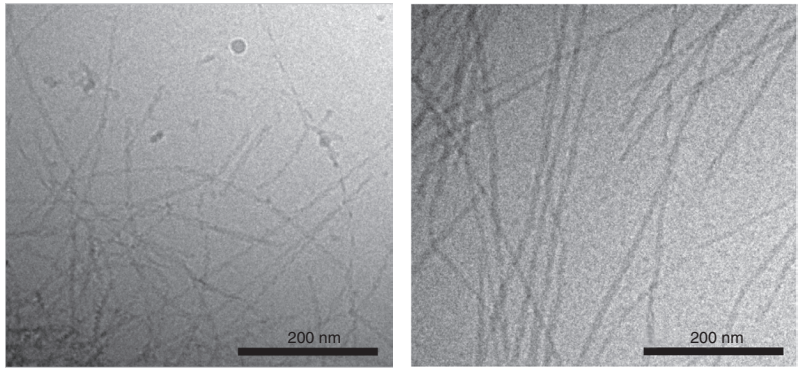

Figure 4 Brichos inhibits the formation of Aβ42 oligomers by suppressing secondary nucleation and redirecting the reaction pathway toward elongation events. (**a**,**b**) Quantification of low-molecular-weight oligomers of Aβ42 in the absence (**a**) or presence (**b**) of Brichos with size-exclusion chromatography and the 6E10 antibody. The reduced intensities of the fractions, verifying the reduction in the population of oligomers due to the chaperone, correspond to the oligomers after incubation times (Δt) of 15, 30, 45 and 60 min. The soluble concentrations of Aβ42 and chaperone were 3 μM, and the concentration of preformed fibrils was 30 nM. (**c**,**d**) Corresponding predictions for the nucleation rate as a function of time with (**d**) and without (**c**) Brichos. (**e**,**f**) Cryo-TEM images of fibrils formed in the absence (**e**) or presence (**f**) of Brichos. The samples contained 10 μM Aβ42 and 6 μM Aβ42 + 6 μM Brichos and were taken at the reaction end point (as measured by thioflavin T) in each case.

studied the interactions between the chaperone and the fibrils by using surface plasmon resonance (SPR) measurements. The data (**Fig. 3b**) reveal that Brichos has a high affinity for the fibrils, whereas it did not bind to SPR sensor surfaces functionalized with monomeric Aβ42 or to reference surfaces lacking any Aβ42; the absence of detectable binding to monomeric Aβ42 (**Fig. 3b**) verifies that the mode of action of Brichos is through interactions with the fibrillar species rather than with soluble monomers. These measurements also provide estimates for the association ($k_{on} \approx 5.1 \times 10^3$ M^{-1} s^{-1}) and dissociation ($k_{off} \approx 2.1 \times 10^{-4}$ s^{-1}) rate constants for the binding of the chaperone to Aβ42 fibrils ($K_d \approx 40$ nM). Remarkably, using these rate constants, we are able to quantitatively and accurately predict (complete derivation of the rate equations in **Supplementary Note**) the experimental kinetic profiles at each of the intermediate concentrations of Brichos tested (**Figure 1c**; predictions shown as thin dotted lines). Moreover, the rate constants predict that under the conditions used to study the effects of preformed seed fibrils, the maximum level of dissociation of Brichos from the seeds prepared in the presence of the chaperone will be only ~68% after 2 h, a finding consistent with the observation (**Fig. 2b**) of a partially reduced catalytic effect of fibrils formed in the presence of Brichos even after several hours.

Brichos blocks the catalytic cycle generating oligomers

The combination of kinetic studies and direct measurements of binding affinity discussed above demonstrate that Brichos is able to bind with high affinity to the surfaces of Aβ42 fibrils. These findings suggest that this molecular chaperone specifically inhibits secondary nucleation events occurring on the surfaces of fibrils. To specifically probe the degree of inhibition of the production of low-molecular-weight oligomeric species created through this mechanism, we studied their concentrations during Aβ42 aggregation in the absence (**Fig. 4a**) and presence (**Fig. 4b**) of Brichos in solution. We monitored the generation of low-molecular-weight oligomeric species in each sample by removing aliquots at a series of time points and isolating in each case the fraction corresponding to low-molecular-weight species by means of size-exclusion chromatography[19]. We pooled eluted fractions into three categories of samples: monomers, small oligomers (trimers to 14-mers, equivalent to globular proteins of 14–65 kDa molecular weight) and large oligomers (15-mers to 20-mers, 66–90 kDa).

We then probed the amount of Aβ42 present in these fractions by using the Aβ42-sensitive 6E10 antibody and observed that the concentration of oligomers was indeed substantially reduced in the presence of Brichos (**Fig. 4a**,**b**). Furthermore, by following the oligomer populations as a function of time, we confirmed that the population of oligomers that is reached during the aggregation process is reduced substantially in the presence of Brichos (**Fig. 4b**), results consistent with our theoretical predictions (**Fig. 4c**,**d**). Thus, through removal of the secondary nucleation process that is normally responsible for the chain reaction that is associated with Aβ42 aggregation, and which results in the rapid generation of oligomeric species[19,29], the reaction

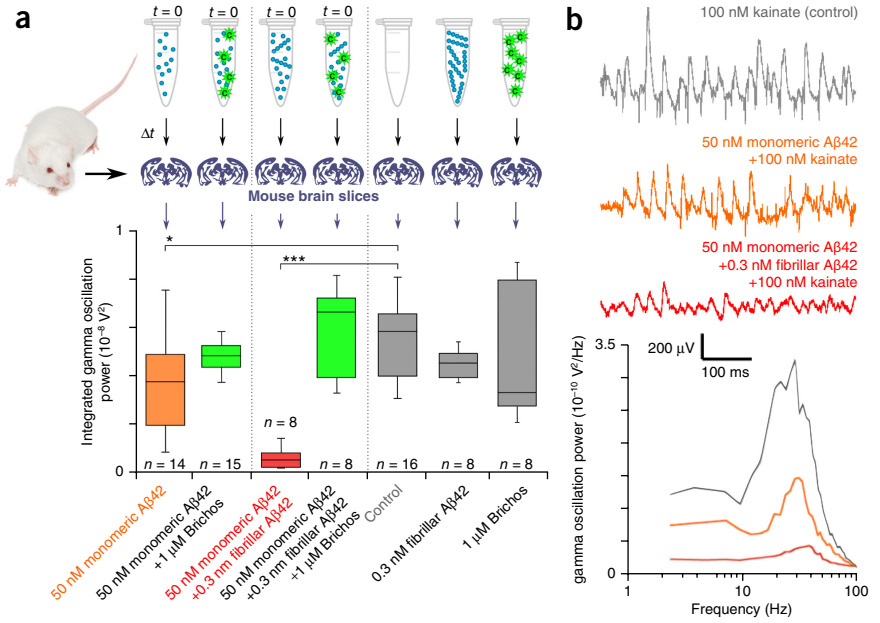

Figure 5 Brichos reduces the toxicity associated with the aggregation of Aβ42 in mouse brain slices. (**a**) Electrophysiology measurements on mouse brain slices, used to measure the degree of Aβ42-induced impairment of hippocampal gamma oscillations in the presence and absence of Brichos. Gray bars, measurements of the control solution and solutions containing mature fibrils alone or chaperone alone. Orange bar, measurements of solutions undergoing aggregation from initially purely monomeric peptide. Red bar, measurements of samples initially containing monomeric Aβ42 with preformed fibrils. Green bars, measurements of solutions undergoing aggregation, both with and without preformed fibrils, to which Brichos was added. The box-and-whisker plot is based on 8–16 repeats for each condition as indicated, with the boxes enclosing data from the first to the third quartile, the horizontal line indicating the median, the whiskers indicating the range and the number of brain slices indicated. $*P = 0.02$; $***P < 0.0001$. All P values are based on two-tailed Mann-Whitney U tests relative to the control. t, time (min). (**b**) Representative traces and power spectra of the kainate-induced gamma oscillation measurements for the control (gray; representative of 16 repeats), the monomeric peptide (orange; representative of 14 repeats) and the monomeric peptide supplemented with preformed fibrils (red; representative of 8 repeats).

pathway is fundamentally modified to generate fibrils from monomers via a reaction network that involves only primary nucleation and elongation and thereby results in the generation of far fewer cytotoxic oligomers. As a consequence of the redirection of the reactive flux away from secondary nucleation and toward elongation events, we observed by cryo-TEM analysis (**Fig. 4e**,**f**) that Aβ42 fibrils formed in the presence of Brichos (**Fig. 4f**) are markedly longer than fibrils formed in the absence of chaperone (**Fig. 4e**). Quantification of the fibril lengths over multiple images revealed that fibrils formed in the presence of Brichos are on average at least four times longer than those formed in the absence of Brichos.

Breaking the catalytic cycle suppresses toxicity in brain tissue

We next analyzed whether or not the reduction in the population of oligomeric species resulting from the specific suppression of the secondary nucleation pathway by Brichos could be sufficient to reduce the high level of neurotoxicity associated with Aβ42 aggregation in brain tissue. To this end, we used electrophysiology techniques on mouse brain slices to measure the degree of Aβ42-induced impairment of hippocampal gamma oscillations in the presence and absence of Brichos (**Fig. 5**). Gamma oscillations are important for higher brain functions such as cognition, learning and memory, and they have been found to be degraded in brain disorders that lead to cognitive decline in patients suffering from neurodegenerative disorders such as Alzheimer's disease[53].

The results reveal that 15-min incubation of samples initially containing only soluble Aβ42 monomers generates limited but significant toxicity (**Fig. 5a**, orange bar, $P = 0.02$) relative to the control, but the addition of small amounts of preformed fibrils to soluble monomers before incubation increases the toxicity significantly at the same time point (**Fig. 5a**, red bar, $P < 0.0001$; representative power spectra in **Fig. 5b**), showing that the toxic species are overwhelmingly produced by fibril-catalyzed processes. Remarkably, in the presence of Brichos (**Fig. 5a**, green bars), such toxicity does not develop, thus confirming that selective inhibition of the pathway generating oligomers dramatically reduces the toxicity associated with Aβ42 aggregation. We observed this reduction in toxicity, to a level comparable with that of the controls, both for reactions initiated from purely monomeric peptide (**Fig. 5a**, first green bar, $P = 0.3$) and for those initiated from solutions including preformed fibrils (**Fig. 5a**, second green bar, $P = 0.2$), demonstrating that the inhibition of secondary nucleation by Brichos reduces toxicity even when Aβ42 fibrils have already been formed. Solutions containing mature fibrils alone and chaperone alone do not show increased toxicity relative to the control (**Fig. 5a**, second and third gray bars, $P = 0.3$ and $P = 0.5$, respectively). We also performed a range of cell-viability and cytotoxicity measurements by MTT and by apoptosis-based assays, respectively, and found consistent trends; critically, in all cases Brichos suppressed the toxicity associated with Aβ42 aggregation, thus leading to readouts close to those of the controls across this range of assays (**Supplementary Fig. 4**).

DISCUSSION

The results that have emerged from this study show that the chaperone Brichos targets a highly specific molecular process in the aggregation pathway of Aβ42: that of fibril-induced secondary nucleation, which is predominantly responsible for the generation of toxic oligomers. Indeed, by inhibiting secondary nucleation, the reaction network underlying the Aβ42 aggregation process (**Fig. 6a**) is fundamentally altered such that the modified pathway leading from monomeric peptide to fibrils proceeds through primary nucleation and elongation-related processes alone (**Fig. 6b**) and results in substantially lower concentrations of toxic oligomers (**Fig. 4b**). The reduction in the population of these species originates from the fact that out of the two processes generating oligomers, primary and secondary nucleation, the chaperone specifically removes the source that is dominant in Aβ42 aggregation[19], namely secondary nucleation (**Fig. 6b**). It is this ability to turn off the otherwise continuing and increasing generation of oligomers through secondary nucleation that explains the efficacy of this process. It is interesting to note, however, that this reduction in oligomer population occurs even though the eventual quantities of

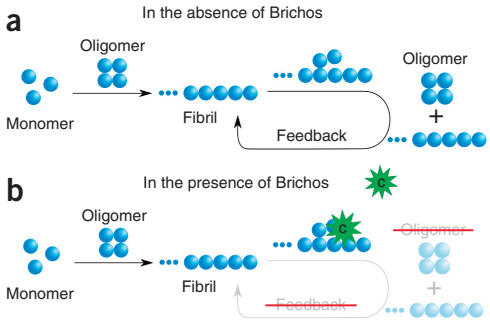

Figure 6 Brichos inhibits the catalytic cycle that generates toxic Aβ42 oligomers. Schematic diagram showing the molecular pathways—primary and secondary nucleation—involved in oligomer formation in Aβ42 aggregation (**a**) and the mechanism by which Brichos suppresses the formation of toxic oligomers, in which the secondary nucleation pathway is specifically inhibited to remove the dominant source of oligomers (**b**).

mature fibrils, which are generated through primary nucleation and elongation alone, remain unaffected by the presence of Brichos[19,20].

The inhibition of secondary pathways identified here represents a mechanism through which a specific molecular chaperone can act to control a single step in the complex process of protein aggregation—in this case, the step that is very largely responsible for the formation of toxic oligomers. This mechanism is effective both in retarding *de novo* aggregation and in delaying aggregation even in the presence of preformed aggregates, and it is therefore an effective means for reducing the toxicity associated with Aβ42 self-assembly at any stage in the process. Most importantly, however, by inhibiting secondary nucleation Brichos is able to dramatically reduce the production of toxic species that otherwise accelerates as the aggregation reaction proceeds. Moreover, because this approach targets the catalytic sites on the fibrils at which secondary nucleation occurs, and does not rely on interactions with the soluble species, it is possible to reach high efficacy even for highly substoichiometric ratios of chaperone to Aβ42 molecules, particularly if the chaperone is able to specifically and preferentially bind to the active catalytic sites rather than to other locations on the fibril surface. Indeed, the identification of Brichos as a specific fibril-binding partner presents a potential approach to establish the precise surface features that permit secondary nucleation.

It is well established that other molecular chaperones are important in assisting in the efficient folding of newly synthesized proteins and in binding to soluble misfolded monomeric or multimeric species to target them for degradation and inhibiting primary nucleation[32–35], the essential first step in the production of aggregates. Our results, however, show that specific chaperones exist that are able to suppress subsequent steps in the process of protein aggregation by inhibiting further proliferation of aggregates, thereby generating a series of protective mechanisms to minimize the risk to an organism of the consequences of misfolding events. In the case of Brichos and Aβ42 aggregation, this step is secondary nucleation, which is responsible for the production of those aggregate species that are most toxic to living cells. Previous observations that a range of other chaperones bind to fibril surfaces[54] suggest that this potent mechanism may be quite general.

This study demonstrates the power of targeting the specific molecular-level processes that are responsible for the toxicity associated with protein aggregation, in contrast to untargeted approaches that focus on the nonspecific suppression of the overall aggregation reaction or processes that do not generate high levels of toxic oligomers. In particular, a reduction in the final fibril load may not be associated with a reduced population of toxic species, thus indicating that molecular chaperones have emerged during biological evolution to have distinctive roles in suppressing specific steps in the process of aggregation. The present results also suggest that strategies designed to identify potential drug targets by screening for suppression of fibril formation may, at least in some cases, lead to compounds that are not able to suppress, or could even increase, the levels of toxic species. Indeed the results show that the populations of cytotoxic oligomers can be successfully reduced without affecting the final fibril load (as shown in **Fig. 1**), and it is interesting to note that this decoupling between the total aggregate load and the observed toxicity could provide a molecular rationalization for the well-established lack of direct correlation between aggregate formation and disease progression[3,6,55–59].

Finally, our findings also reveal that elucidating the specific molecular processes by which toxicity occurs is a vital step in understanding the nature of biological defense mechanisms, and hence it may potentially be important in the rational design of effective therapeutic strategies to combat Alzheimer's disease. Moreover, given the existence of common features of the mechanisms of protein aggregation[2,7], such approaches are likely to be important for addressing misfolding diseases more generally. Indeed, our results suggest that nature has evolved this type of targeted strategy for suppressing toxicity through molecular chaperones that are capable of not only promoting the folding and suppressing the misfolding of proteins in solution but also selectively interfering in the different steps in the complex reaction pathways associated with peptide and protein aggregation and, in the case of Brichos studied here, blocking the catalytic production of toxic species.

METHODS

Methods and any associated references are available in the online version of the paper.

Note: Any Supplementary Information and Source Data files are available in the online version of the paper.

ACKNOWLEDGMENTS

We acknowledge financial support from the Schiff Foundation (S.I.A.C.), the Swedish Research Council (S.L., J.J. and J.P.) and its Linneaus Centre Organizing Molecular Matter (S.L.), the Crafoord Foundation (S.L.), Alzheimerfonden (S.L.), the Frances and Augustus Newman Foundation (P.A. and T.P.J.K.), the European Research Council (T.P.J.K. and S.L.), the Biotechnology and Biological Sciences Research Council (T.P.J.K.), the Nanometer Structure Consortium at Lund University (S.L.), the KID PhD studentship grant (F.R.K. and L.D.), the Swedish Medical Association (A.F.), the Brain Fund (A.F.), the Strategic Program in Neurosciences at the Karolinska Institutet (A.F.), the Swiss National Science Foundation (P.A.) and the Wellcome Trust (C.M.D. and T.P.J.K.). We thank T. Weaver (University of Cincinnati) for reagents.

AUTHOR CONTRIBUTIONS

S.I.A.C., T.P.J.K., A.F. and S.L. designed the study. J.P., F.R.K., A.F., L.D., C.D., X.Y., B.F., H.B. and S. L. performed the experiments. S.I.A.C., P.A., T.P.J.K., F.R.K., C.M.D., A.F. and S.L. analyzed the data. S.I.A.C., P.A., C.M.D., T.P.J.K. and S.L. wrote the paper. All authors discussed the results and commented on the manuscript.

COMPETING FINANCIAL INTERESTS

The authors declare no competing financial interests.

1. Aguzzi, A. & O'Connor, T. Protein aggregation diseases: pathogenicity and therapeutic perspectives. *Nat. Rev. Drug Discov.* **9**, 237–248 (2010).
2. Dobson, C.M. Protein folding and misfolding. *Nature* **426**, 884–890 (2003).

3. Haass, C. & Selkoe, D.J. Soluble protein oligomers in neurodegeneration: lessons from the Alzheimer's amyloid β-peptide. *Nat. Rev. Mol. Cell Biol.* **8**, 101–112 (2007).
4. Selkoe, D.J. Folding proteins in fatal ways. *Nature* **426**, 900–904 (2003).
5. Tanzi, R.E. & Bertram, L. Twenty years of the Alzheimer's disease amyloid hypothesis: a genetic perspective. *Cell* **120**, 545–555 (2005).
6. Chiti, F. & Dobson, C.M. Protein misfolding, functional amyloid, and human disease. *Annu. Rev. Biochem.* **75**, 333–366 (2006).
7. Knowles, T.P.J., Vendruscolo, M. & Dobson, C.M. The amyloid state and its association with protein misfolding diseases. *Nat. Rev. Mol. Cell Biol.* **15**, 384–396 (2014).
8. Sipe, J.D. *et al.* Amyloid fibril protein nomenclature: 2012 recommendations from the nomenclature committee of the International Society of Amyloidosis. *Amyloid* **19**, 167–170 (2012).
9. Goldschmidt, L., Tenga, P.K., Riek, R. & Eisenberg, D. Identifying the amylome, proteins capable of forming amyloid-like fibrils. *Proc. Natl. Acad. Sci. USA* **107**, 3487–3492 (2010).
10. Greenwald, J. & Riek, R. Biology of amyloid: structure, function, and regulation. *Structure* **18**, 1244–1260 (2010).
11. Koo, E.H., Lansbury, P.T. Jr. & Kelly, J.W. Amyloid diseases: abnormal protein aggregation in neurodegeneration. *Proc. Natl. Acad. Sci. USA* **96**, 9989–9990 (1999).
12. Bucciantini, M. *et al.* Inherent toxicity of aggregates implies a common mechanism for protein misfolding diseases. *Nature* **416**, 507–511 (2002).
13. Kayed, R. *et al.* Common structure of soluble amyloid oligomers implies common mechanism of pathogenesis. *Science* **300**, 486–489 (2003).
14. Walsh, D.M. *et al.* Naturally secreted oligomers of amyloid β protein potently inhibit hippocampal long-term potentiation *in vivo*. *Nature* **416**, 535–539 (2002).
15. Collins, S.R., Douglass, A., Vale, R.D. & Weissman, J.S. Mechanism of prion propagation: amyloid growth occurs by monomer addition. *PLoS Biol.* **2**, e321 (2004).
16. Jarrett, J.T. & Lansbury, P.T. Jr. Seeding "one-dimensional crystallization" of amyloid: a pathogenic mechanism in Alzheimer's disease and scrapie? *Cell* **73**, 1055–1058 (1993).
17. Knowles, T.P.J. *et al.* An analytical solution to the kinetics of breakable filament assembly. *Science* **326**, 1533–1537 (2009).
18. Cremades, N. *et al.* Direct observation of the interconversion of normal and toxic forms of α-synuclein. *Cell* **149**, 1048–1059 (2012).
19. Cohen, S.I.A. *et al.* Proliferation of amyloid-beta42 aggregates occurs through a secondary nucleation mechanism. *Proc. Natl. Acad. Sci. USA* **110**, 9758–9763 (2013).
20. Hellstrand, E., Boland, B., Walsh, D.M. & Linse, S. Amyloid β-protein aggregation produces highly reproducible kinetic data and occurs by a two-phase process. *ACS Chem. Neurosci.* **1**, 13–18 (2010).
21. Lee, J., Culyba, E.K., Powers, E.T. & Kelly, J.W. Amyloid-β forms fibrils by nucleated conformational conversion of oligomers. *Nat. Chem. Biol.* **7**, 602–609 (2011).
22. Serio, T.R. *et al.* Nucleated conformational conversion and the replication of conformational information by a prion determinant. *Science* **289**, 1317–1321 (2000).
23. Kar, K., Jayaraman, M., Sahoo, B., Kodali, R. & Wetzel, R. Critical nucleus size for disease-related polyglutamine aggregation is repeat-length dependent. *Nat. Struct. Mol. Biol.* **18**, 328–336 (2011).
24. Oosawa, F. & Asakura, S. *Thermodynamics of the Polymerization of Protein* (Academic Press, 1975).
25. Ferrone, F.A., Hofrichter, J. & Eaton, W.A. Kinetics of sickle hemoglobin polymerization. II. A double nucleation mechanism. *J. Mol. Biol.* **183**, 611–631 (1985).
26. Cohen, S.I.A., Vendruscolo, M., Dobson, C.M. & Knowles, T.P.J. Nucleated polymerization with secondary pathways. II. Determination of self-consistent solutions to growth processes described by non-linear master equations. *J. Chem. Phys.* **135**, 065106 (2011).
27. Ruschak, A.M. & Miranker, A.D. Fiber-dependent amyloid formation as catalysis of an existing reaction pathway. *Proc. Natl. Acad. Sci. USA* **104**, 12341–12346 (2007).
28. Arosio, P., Cukalevski, R., Frohm, B., Knowles, T.P.J. & Linse, S. Quantification of the concentration of Aβ42 propagons during the lag phase by an amyloid chain reaction assay. *J. Am. Chem. Soc.* **136**, 219–225 (2014).
29. Jeong, J.S., Ansaloni, A., Mezzenga, R., Lashuel, H.A. & Dietler, G. Novel mechanistic insight into the molecular basis of amyloid polymorphism and secondary nucleation during amyloid formation. *J. Mol. Biol.* **425**, 1765–1781 (2013).
30. Salvadores, N., Shahnawaz, M., Scarpini, E., Tagliavini, F. & Soto, C. Detection of misfolded Aβ oligomers for sensitive biochemical diagnosis of Alzheimer's disease. *Cell Rep.* **7**, 261–268 (2014).
31. Willander, H. *et al.* Brichos domains efficiently delay fibrillation of amyloid beta-peptide. *J. Biol. Chem.* **287**, 31608–31617 (2012).
32. Hartl, F.U. Molecular chaperones in cellular protein folding. *Nature* **381**, 571–579 (1996).
33. Hartl, F.U., Bracher, A. & Hayer-Hartl, M. Molecular chaperones in protein folding and proteostasis. *Nature* **475**, 324–332 (2011).
34. Kim, Y.E., Hipp, M.S., Bracher, A., Hayer-Hartl, M. & Hartl, F.U. Molecular chaperone functions in protein folding and proteostasis. *Annu. Rev. Biochem.* **82**, 323–355 (2013).
35. Balch, W.E., Morimoto, R.I., Dillin, A. & Kelly, J.W. Adapting proteostasis for disease intervention. *Science* **319**, 916–919 (2008).
36. Doyle, S.M., Genest, O. & Wickner, S. Protein rescue from aggregates by powerful molecular chaperone machines. *Nat. Rev. Mol. Cell Biol.* **14**, 617–629 (2013).
37. Auluck, P.K., Chan, H.Y.E., Trojanowski, J.Q., Lee, V.M.Y. & Bonini, N.M. Chaperone suppression of alpha-synuclein toxicity in a *Drosophila* model for Parkinson's disease. *Science* **295**, 865–868 (2002).
38. Bence, N.F., Sampat, R.M. & Kopito, R.R. Impairment of the ubiquitin-proteasome system by protein aggregation. *Science* **292**, 1552–1555 (2001).
39. Morimoto, R.I. Proteotoxic stress and inducible chaperone networks in neurodegenerative disease and aging. *Genes Dev.* **22**, 1427–1438 (2008).
40. Sakahira, H., Breuer, P., Hayer-Hartl, M.K. & Hartl, F.U. Molecular chaperones as modulators of polyglutamine protein aggregation and toxicity. *Proc. Natl. Acad. Sci. USA* **99** (suppl. 4), 16412–16418 (2002).
41. Schaffar, G. *et al.* Cellular toxicity of polyglutamine expansion proteins: mechanism of transcription factor deactivation. *Mol. Cell* **15**, 95–105 (2004).
42. Månsson, C. *et al.* Interaction of the molecular chaperone DNAJB6 with growing amyloid-beta 42 (Aβ42) aggregates leads to sub-stoichiometric inhibition of amyloid formation. *J. Biol. Chem.* **289**, 31066–31076 (2014).
43. Sánchez-Pulido, L., Devosi, D. & Valencia, A. Brichos: a conserved domain in proteins associated with dementia, respiratory distress and cancer. *Trends Biochem. Sci.* **27**, 329–332 (2002).
44. Hedlund, J., Johansson, J. & Persson, B. Brichos: a superfamily of multidomain proteins with diverse functions. *BMC Res. Notes* **2**, 180 (2009).
45. Knight, S.D., Presto, J., Linse, S. & Johansson, J. The brichos domain, amyloid fibril formation, and their relationship. *Biochemistry* **52**, 7523–7531 (2013).
46. Willander, H., Hermansson, E., Johansson, J. & Presto, J. Brichos domain associated with lung fibrosis, dementia and cancer: a chaperone that prevents amyloid fibril formation? *FEBS J.* **278**, 3893–3904 (2011).
47. Nerelius, C., Gustafsson, M., Nordling, K., Larsson, A. & Johansson, J. Anti-amyloid activity of the c-terminal domain of prosp-c against amyloid beta-peptide and medin. *Biochemistry* **48**, 3778–3786 (2009).
48. Coomaraswamy, J. *et al.* Modeling familial Danish dementia in mice supports the concept of the amyloid hypothesis of Alzheimer's disease. *Proc. Natl. Acad. Sci. USA* **107**, 7969–7974 (2010).
49. Kim, J. *et al.* Bri2 (itm2b) inhibits Aβ deposition *in vivo*. *J. Neurosci.* **28**, 6030–6036 (2008).
50. Vidal, R. *et al.* A stop-codon mutation in the *BRI* gene associated with familial British dementia. *Nature* **399**, 776–781 (1999).
51. Willander, H. *et al.* High-resolution structure of a brichos domain and its implications for anti-amyloid chaperone activity on lung surfactant protein c. *Proc. Natl. Acad. Sci. USA* **109**, 2325–2329 (2012).
52. Cohen, S.I.A. *et al.* Nucleated polymerization with secondary pathways. I. Time evolution of the principal moments. *J. Chem. Phys.* **135**, 065105 (2011).
53. Schnitzler, A. & Gross, J. Normal and pathological oscillatory communication in the brain. *Nat. Rev. Neurosci.* **6**, 285–296 (2005).
54. Knowles, T.P.J. *et al.* Role of intermolecular forces in defining material properties of protein nanofibrils. *Science* **318**, 1900–1903 (2007).
55. Lue, L.F. *et al.* Soluble amyloid beta peptide concentration as a predictor of synaptic change in Alzheimer's disease. *Am. J. Pathol.* **155**, 853–862 (1999).
56. McLean, C.A. *et al.* Soluble pool of Aβ amyloid as a determinant of severity of neurodegeneration in Alzheimer's disease. *Ann. Neurol.* **46**, 860–866 (1999).
57. Näslund, J. *et al.* Correlation between elevated levels of amyloid beta-peptide in the brain and cognitive decline. *J. Am. Med. Assoc.* **283**, 1571–1577 (2000).
58. Wang, J., Dickson, D.W., Trojanowski, J.Q. & Lee, V.M. The levels of soluble versus insoluble brain Aβ distinguish Alzheimer's disease from normal and pathologic aging. *Exp. Neurol.* **158**, 328–337 (1999).
59. Hermansson, E. *et al.* The chaperone domain BRICHOS prevents CNS toxicity of amyloid-β peptide in *Drosophila melanogaster*. *Dis. Model. Mechl.* **7**, 659–665 (2014).

ONLINE METHODS

Materials. We expressed the Aβ(M1–42) peptide (MDAEFRHDSGYEVHHQ KLVFFAEDVGSNKGAIIGLMVGGVVIA) in *Escherichia coli* from a synthetic gene and purified the peptide essentially as described previously[60]. In short, the purification procedure involved sonication of *E. coli* cells, dissolution of inclusion bodies in 8 M urea, ion exchange in batch mode on DEAE cellulose resin, lyophilization and gel filtration on a 3.4 cm × 200 cm gel-filtration column at 4 °C. The purified peptide was frozen as identical 3-mL aliquots and lyophilized. proSP-C Brichos was expressed in *E. coli* and purified as described previously[31]. Purification of the control proteins was as described elsewhere for human calmodulin[61], fatty acid–free human serum albumin[62], bovine calbindin D9k[63] and the B1 domain of streptococcal protein G[64].

Kinetic assays. For kinetic experiments, aliquots of purified Aβ42 were dissolved in 6 M GuHCl, and the monomer was isolated by two rounds of gel filtration on a Superdex 75 column in 20 mM sodium phosphate buffer, pH 8, with 200 μM EDTA and 0.02% NaN_3. The center of the monomer peak was collected on ice and lyophilized. The sample was again dissolved in 6 M GuHCl, and the monomer, isolated by gel filtration on a Superdex 75 column in 20 mM sodium phosphate buffer, pH 8, with 200 μM EDTA and 0.02% NaN_3, was typically found to have a concentration (determined by quantitative amino acid analysis purchased from BMC Uppsala) of 5–12 μM. The gel-filtration step removes traces of preexisting aggregates and exchanges the buffer to the one used in the fibril formation experiments. The monomer generated in this way was diluted with buffer, or with buffer and Brichos, and supplemented with 6 μM thioflavin T (ThT) from a 1.2 mM stock to prepare a series of samples with the same Aβ42 concentration but different Brichos concentrations. All samples were prepared in low-bind Eppendorf tubes (Axygen) on ice by careful pipetting to avoid introduction of air bubbles. Each sample was then pipetted into multiple wells of a 96-well half-area plate of black polystyrene with a clear bottom and PEG coating (Corning 3881), 100 μL per well. Assays were initiated by placing the 96-well plate at 37 °C in a plate reader (Fluostar Omega, Fluostar Optima or Fluostar Galaxy, BMGLabtech). A series of control experiments[19,20] demonstrated that under the conditions used, the fluorescence from ThT is linearly related to the Aβ42 aggregate mass concentration.

Kinetic assays with preformed fibrils. Kinetic experiments were set up as above for multiple samples of Aβ42 in 20 mM sodium phosphate buffer, pH 8, with 200 μM EDTA, 6 μM ThT and 0.02% NaN_3. The fluorescence of added ThT was monitored for 1.5 h to verify the formation of fibrils. The samples were then collected from the wells into low-bind Eppendorf tubes (Axygen) and sonicated for 2 min in a sonicator bath at room temperature to disrupt any fibril clusters. Fresh monomer was isolated by gel filtration as above and diluted to 3 μM, with or without 3 μM Brichos in 20 mM sodium phosphate, pH 8, containing 200 μM EDTA, 6 μM ThT and 0.02% NaN_3. Samples were prepared containing the sonicated preformed fibrillar seeds at concentrations corresponding to 0%, 0.04%, 0.2% and 1% of the highest monomer concentration in the dilution series, and therefore the concentration of Brichos remaining in solution with the preformed fibrils was below 0.03 μM. The ThT fluorescence was monitored in the plate reader every 60 s under quiescent conditions at 37 °C. The previously established rate constants[19] for elongation and secondary nucleation in Aβ42 aggregation show that at the concentrations of preformed fibrils applied here, the accelerating effect on the reaction is due primarily to secondary nucleation events catalyzed by the surfaces of the added fibrils rather than to elongation processes induced by the added reactive fibril ends, a conclusion verified in **Figure 2c,d**, in which secondary nucleation is inhibited.

Kinetic rate laws. From our previous analyses[19,26], the generation of fibril mass, M, when both primary and secondary nucleation events occur, is described by the integrated rate law

$$\frac{M(t)}{M(\infty)} = 1 - \left(\frac{B_+ + C_+}{B_+ + C_+ e^{\kappa t}} \frac{B_- + C_+ e^{\kappa t}}{B_- + C_+} \right)^{\frac{k_\infty 2}{\kappa \tilde{k}_\infty}} e^{-k_\infty t} \qquad (1)$$

in which two particular combinations of the rate constants for primary nucleation (k_n), elongation (k_+) and fibril-catalyzed secondary nucleation (k_2) define much of the macroscopic behavior; these parameters are related to the rate of formation of new aggregates through primary pathways

$$\lambda = \sqrt{2k_+ k_n m(0)^{n_c}}$$

and through secondary pathways

$$\kappa = \sqrt{2k_+ k_2 m(0)^{n_2 + 1}}$$

Indeed, equation (1) depends on the rate constants through these two parameters, λ and κ alone, because $B_\pm = (k_\infty \pm \tilde{k}_\infty)/(2\kappa)$, $C_\pm = \pm \lambda^2/(2\kappa^2)$,

$$k_\infty = \sqrt{2\kappa^2/[n_2(n_2+1)] + 2\lambda^2/n_c}$$

and

$$\tilde{k}_\infty = \sqrt{k_\infty^2 - 4C_+C_-\kappa^2}$$

The initial concentration of soluble monomers is denoted $m(0)$, and the exponents describing the dependencies of the primary and secondary pathways on the monomer concentration are given as n_c and n_2, respectively.

The effect of an inhibitor can in the first instance be semiempirically captured by altering the microscopic rate constants for primary nucleation (k_n), elongation (k_+) and secondary nucleation (k_2) in the integrated rate law in equation (1). Perturbing the different microscopic events results in characteristic changes in the shape of the macroscopic reaction profile that can be used to identify the mechanism of action of an inhibitor (**Fig. 1a–c**). This approach is exact for complete inhibition of a particular process, as shown for secondary nucleation in **Figure 1c** (green dashed line). Using this approach (**Fig. 1a–c** and **Supplementary Fig. 2**), we were able to identify a Brichos domain that specifically affects the secondary nucleation rate.

In order to further quantify the inhibitory effect of the Brichos domain at chaperone concentrations at which inhibition of secondary nucleation is not complete and to predict the kinetic profiles at intermediate chaperone concentrations (thin dotted lines, **Fig. 1c**), we then used a first-principles approach by introducing into the reaction scheme the reversible binding of the chaperone along the fibril surface. Such binding decreases the surface of the fibrils available to catalyze the oligomer formation, therefore reducing the secondary nucleation rate. A complete derivation of the rate equations including this Langmuir-type adsorption mechanism is provided in **Supplementary Note**.

Transmission electron microscopy. Samples from the kinetic experiments were taken at the end point of the experiment (ThT maximum) for reactions involving Aβ42 alone and reactions involving Aβ42 together with 0.7 equivalents of Brichos. Aliquots of 2-μL volume were loaded on nickel-coated grids, and any excess sample was removed. The grids were placed on a drop of 1% BSA in TBS, incubated for 30 min at room temperature and then washed three times for 10 min with TBS. The grids were then placed on drops of rabbit anti–C-terminal proSP-C (kindly provided by T. Weaver[65]) that was diluted 1:200 in TBS and incubated overnight at 4 °C. After being washed five times for 10 min, the grids were placed on goat anti-rabbit IgG coupled to 10-nm gold particles (BBI Solutions, EM.GAR10) that was diluted 1:40 in TBS and were incubated for 2 h at room temperature. The grids were then washed five times as before; this was followed by negative staining with 2% uranyl acetate in 50% ethanol and examination of the immunolabeled fibrils with a Hitachi H7100 TEM operated at 75 kV.

Cryogenic transmission electron microscopy. To ensure a stable temperature and to avoid the loss of solution during sample preparation, a controlled-environment vitrification system was used. Samples were prepared as thin liquid films (<300 nm thick) on glow discharge–treated lacey carbon film–coated copper grids and plunged into liquid ethane at −180 °C. In this way, the original microstructures are preserved as component segmentation and rearrangement in addition to water crystallization are avoided as the samples are vitrified. Samples were stored under liquid N_2 until measurement and were then transferred with an Oxford CT3500 cryoholder and its workstation into the electron microscope (Philips CM120 BioTWIN Cryo) equipped with a postcolumn energy filter (Gatan GIF100). An acceleration voltage of 120 kV

doi:10.1038/nsmb.2971

was used, and images were recorded digitally with a CCD camera under low-electron-dose conditions. The lengths of approximately 150 fibrils across multiple images were measured with Digital Micrograph software. For the case of Aβ42 in the presence of Brichos, many fibrils were so long as to have one end outside the field of view of our images, and those were excluded from the analysis. By contrast, several of the fibrils formed in the absence of Brichos were too short and tangled with one another to be measured accurately and were likewise excluded. The reported ratio of the average length of fibrils formed in the presence of Brichos to that in the absence of Brichos is hence to be taken as a lower bound for its exact value.

Surface plasmon resonance assays. Aβ42 monomers or fibrils were immobilized on C1 sensor chips (GE Healthcare) with amine coupling. A fresh mixture of 0.05 M NHS and 0.2 M EDC was added to the sensor-chip surface for activation; this was followed by washing and incubation with 1 μM Aβ42 monomers or fibrils outside of the instrument at room temperature for 0.5 and 2.0 h, respectively, and finally blocking by ethanolamine. Blank channels for negative controls were prepared by omitting protein in the coupling step. Binding of Brichos was measured with a BIACORE 3000 instrument by injection of 100 μL of a 1 μM solution of proSP-C Brichos and subsequent buffer flow to monitor dissociation. The flow rate was 10 μL/min throughout the experiment.

Monomer and oligomer fraction analysis with monoclonal antibodies. Aggregation was monitored by ThT fluorescence for samples of 5 μM Aβ42 with 50 nM of preformed seeds with and without 5 μM pro-SPC Brichos in 20 mM sodium phosphate buffer, pH 8, with 200 μM EDTA and 0.02% NaN_3 with 6 μM ThT. Samples were taken from reactions without Brichos after 15 min, and from reactions with Brichos after 15, 30, 45 and 60 min (**Fig. 4**). The samples were collected from the wells and immediately injected into a 1 × 30 cm Superdex 75 column. Eluted fractions (1 mL per fraction) were pooled in three samples: monomers (elution volume between 11.5 and 15 ml), small oligomers (elution volume between 8 and 11.5 ml) and large oligomers (elution volume between 5 and 8 ml). According to the calibration curve of the SEC column performed with globular proteins, small and large oligomers correspond to species with molecular weights in the range 14–65 kDa (trimers to 14-mers) and 66–90 kDa (15-mers to 20-mers) equivalent of globular proteins, respectively, with dimers eluting in the tail of the monomer peak. Pooled samples were pulled through a PVDF membrane (200 nm) with a vacuum device for semiquantitative analysis with a 6E10 primary mouse antibody (Signet SIG-39300) and goat anti-mouse secondary antibody (Dako, R048001-2) conjugated with an IR probe (LICOR 929-09406) and fluorescence detection after excitation at 800 nm in a LI-COR Odyssey CLx instrument.

Electrophysiology. Experiments were carried out in accordance with an ethical permit granted to A.F. by Norra Stockholms Djurförsöksetiska Nämnd (N45/13). C57BL/6 mice of either sex (postnatal days 14–23, supplied from Charles River) were used in all experiments. No statistical method was used to predetermine the sample size of 8–16 per group, which was chosen on the basis of previous experiments. The experiments were not randomized and were not performed with blinding to the conditions of the experiments. Immediately after being sliced, sections were transferred to a submerged incubation chamber containing standard artificial cerebrospinal fluid (ACSF): 124 mM NaCl, 30 mM $NaHCO_3$, 10 mM glucose, 1.25 mM NaH_2PO_4, 3.5 mM KCl, 1.5 $MgCl_2$ and 1.5 mM $CaCl_2$. The chamber was held at 34 °C for at least 20 min after dissection. It was subsequently allowed to cool to ambient room temperature (19–22 °C) for a minimum of 40 min. Aβ42 monomer was at 5–10 μM; it was isolated by gel filtration in 20 mM sodium phosphate buffer, pH 8.0, and was subsequently filtered through a 200-nm sterile filter and stored on ice until use. Fibrils were prepared by incubation of a 5 μM Aβ42 solution in a nonbinding plate at 37 °C for 1 h under quiescent conditions. Peptides (final concentration 50 nM monomer or 50 nM monomer plus 0.3 nM fibrils) were added to the incubation solution 15 min before slices were transferred to the interface-style recording chamber. During incubation, slices were continuously supplied with carbogen gas (5% CO_2 and 95% O_2) bubbled into the ACSF. Recordings were carried out in hippocampal area CA3 with borosilicate glass microelectrodes pulled to a resistance of 3–7 MΩ. Local field potentials (LFPs) were recorded at 34 °C with microelectrodes filled with artificial cerebrospinal fluid placed in stratum pyramidale. LFP oscillations were elicited by application of kainic acid (100 nM) to the extracellular bath. The signals were sampled at 10 kHz with conditioning with a Hum Bug 50 Hz noise eliminator (Quest Scientific), software low-pass-filtered at 1 kHz, and digitized and stored with a Digidata 1322A and Clampex 9.6 software (Molecular Devices). Power spectral density plots (from 60-s-long LFP recordings) were calculated in averaged Fourier segments of 8,192 points with Axograph X (Kagi). The oscillation power was calculated by integration of the power spectral density between 20 and 80 Hz. For statistical analysis, the Mann-Whitney *U* test was used. Full experimental protocols are provided in the **Supplementary Note**.

Cell viability and cytotoxicity. Cell viability was measured with an MTS reagent, and cytotoxicity was measured with caspase-3/7 activity. These assays are commonly used, although the analysis is less straightforward compared to that of the electrophysiology experiments. Both assays suffer from the limitation that the single colorimetric readout represents the global effect of many possible cellular processes. For example, an increase of caspase signal is commonly associated with an increase of apoptosis activity of the cells, although caspase activation has been observed in the absence of apoptosis[66]. Assays were performed on SHSY-5Y human neuroblastoma cells cultured under standard conditions at 37 °C in a humidified incubator with 5% CO_2. Cells were seeded at a density of 25,000 per well in a white-walled, clear-bottomed 96-well plate and cultured for 24 h in DMEM/10% FBS. The culture medium was then replaced with prewarmed phenol red–free DMEM without serum into which the peptide samples or NaH_2PO_4 buffer were diluted 1:4. Peptide monomer was isolated by gel filtration in 20 mM sodium phosphate buffer at pH 8.0; this was followed by filtration through a 200-nm sterile filter and storage on ice until addition to the cells. Seeds were prepared by incubation of a monomer solution in a 96-well nonbinding plate (Corning 3881) at 37 °C for 1 h. Completion of fibril formation was confirmed by ThT fluorescence on a withdrawn aliquot. Seeds were then diluted 1:100 into fresh monomer. The experiments for monomer and monomer plus seeds were repeated in the presence of Brichos. Buffer and Brichos were filtered through a 200-nm sterile filter. The cells were cultured in the presence of the peptides or buffer (five-fold diluted in medium) for a further 24 h before the cytotoxicity and viability assays were performed. Caspase-3/7 activity was measured with the Apo-ONE Homogeneous Caspase-3/7 assay (Promega). The fluorogenic caspase-3/7 substrate was diluted 1:100 in the lysis buffer provided and added to the cell medium at a 1:1 ratio. The reagent/cell mix was then incubated for 1 h before measurement of the fluorescence at ex. 480 nm/em. 520 nm in an Optima FluoStar plate reader. Cell viability was measured with the Cell Titer 96 Aqueous One MTS reagent from Promega. The MTS reagent was added to the cell-culture medium and incubated with the cells at 37 °C in a humidified incubator with 5% CO_2 before the absorbance at 495 nm was measured in an Optima Fluostar plate reader. All values given for both assays are normalized relative to the buffer-treated cells. Additional experimental details are provided in the **Supplementary Note**.

60. Walsh, D.M. *et al.* A facile method for expression and purification of the Alzheimer's disease-associated amyloid beta-peptide. *FEBS J.* **276**, 1266–1281 (2009).
61. Waltersson, Y., Linse, S., Brodin, P. & Grundström, T. Mutational effects on the cooperativity of Ca2 binding in calmodulin. *Biochemistry* **32**, 7866–7871 (1993).
62. Cedervall, T. *et al.* Understanding the nanoparticle-protein corona using methods to quantify exchange rates and affinities of proteins for nanoparticles. *Proc. Natl. Acad. Sci. USA* **104**, 2050–2055 (2007).
63. Johansson, C. *et al.* Biophysical studies of engineered mutant proteins based on calbindin D9k modified in the pseudo EF-hand. *Eur. J. Biochem.* **187**, 455–460 (1990).
64. Lindman, S. *et al.* Salting the charged surface: pH and salt dependence of protein G B1 stability. *Biophys. J.* **90**, 2911–2921 (2006).
65. Johansson, H. *et al.* The Brichos domain-containing C-terminal part of pro-surfactant protein C binds to an unfolded poly-val transmembrane segment. *J. Biol. Chem.* **281**, 21032–21039 (2006).
66. Burguillos, M.A. *et al.* Caspase signalling controls microglia activation and neurotoxicity. *Nature* **472**, 319–324 (2011).